Noncompact lattice QED with two charges: Phase diagram and renormalization group flow

A. Ali Khan
Department of Physics and Astronomy, University of Glasgow, Glasgow G12 8QQ, United Kingdom
(Received 13 November 1995)

The phase diagram of noncompact lattice QED in four dimensions with staggered fermions of charges 1 and $-1/2$ is investigated. The renormalized charges are determined and found to be in agreement with perturbation theory. This is an indication that there is no continuum limit with nonvanishing renormalized gauge coupling, and that the theory has a validity bound for every finite value of the renormalized coupling. The renormalization group flow of the charges is investigated and an estimate for the validity bound as a function of the cutoff is obtained. Generalizing this estimate to all fermions in the standard model, it is found that a cutoff at the Planck scale implies that α_R has to be less than 1/80. Because of spontaneous chiral symmetry breaking, strongly bound fermion-antifermion composite states are generated. Their spectrum is discussed. [S0556-2821(96)05609-3]

PACS number(s): 11.15.Ha, 11.10.Hi, 12.20.Ds

I. INTRODUCTION

Interest in nonperturbative investigations of QED has a long history. From perturbation theory there are indications (Landau pole [1]) that the cutoff can only be removed from the theory if the renormalized charge vanishes. Also, it is a yet-unsolved fundamental question [2] why the fine structure constant has the value $\alpha \simeq 1/137$. At strong coupling, QED exhibits a chiral symmetry-breaking phase transition of second order [3–6], where tightly bound fermion-antifermion pairs are generated. There one could expect a deviation from the charge screening behavior known from perturbative QED. The phase transition makes strongly coupled U(1) gauge theories interesting also for applications in technicolor theories because of large anomalous dimensions of the operator $\bar{\psi}\psi$ [7]. For several years, the possibility of a nontrivial continuum limit, or a nontrivial ultraviolet-stable fixed point of the Callan-Symanzik β function, has been investigated in the noncompact formulation of QED on the lattice (see, for example, [9–16]).

Studying noncompact lattice QED with dynamical fermions, some groups find nontrivial scaling behavior [12,17,18], while others find their critical exponents to indicate triviality [13,19]. The QED β function has been studied nonperturbatively on the lattice [15,20], and by using Schwinger-Dyson equations [21]. It turns out to be in agreement with perturbation theory, and it shows no indication of a nontrivial fixed point. If QED is trivial in the limit of infinite cutoff, there is a maximal cutoff corresponding to every finite value of the renormalized charge. One is interested in the size of this validity bound. A rough estimate of it has been made in a lattice study of QED with one charge [15].

In nature one finds several differently charged types of fermions. In the presence of several charges, new nonperturbative phenomena may arise which could affect the phase structure. An important question is whether chiral symmetry breaking sets in at the same value of the bare coupling for all fermions or whether some fermion species can be massless and others in the chirally broken phase at the same time. The phase diagram of such a system has to be investigated with respect to a physically interesting continuum limit. In QED with one charge, neutral pointlike Goldstone bosons and scalar particles are generated due to the chiral symmetry-breaking phase transition. One could expect that in the two-charge model there is a larger number of neutral pointlike bound states which could, in principle, carry color charge and have an effect on the β function of QCD. Moreover, electrically charged bound states may appear which could change the behavior of the QED β function and push the validity bound towards much lower energies. It is of interest to see whether charge renormalization is in agreement with perturbation theory and which states give relevant contributions.

To investigate nonperturbative phenomena in the coupling between different species of fermions, a model with two species of staggered fermions with a ratio of their charges of $-1/2$ (''two-charge model'') was studied, comparable to u and d quarks whose strong and weak interactions are switched off.

In Sec. II of this paper a description of the model and details of the simulation are given. The phase diagram, obtained from the chiral condensates, and the scaling behaviour are discussed. The charged sector of the model is presented in Sec. III. The renormalized charges are determined nonperturbatively using current-photon correlation functions and are compared with renormalized lattice perturbation theory. There is a good agreement which leads to the conclusion that the model is trivial. Using perturbation theory, the renormalization group flow of the charges is determined, which leads to an estimate of the validity bound resulting from triviality. Spectrum and renormalization group flows of fermion-antifermion composite states are discussed in Sec. IV. The conclusions are given in Sec. V.

II. PHASE DIAGRAM AND SCALING BEHAVIOR

A. Action and simulation details

The ''two-charge model'' contains a noncompact gauge field with the action

$$S_g = \frac{\beta}{2} \sum_x \sum_{\mu<\nu} F_{\mu\nu}^2(x), \tag{1}$$

$$F_{\mu\nu}(x) = \Delta_\mu A_\nu(x) - \Delta_\nu A_\mu(x), \tag{2}$$

TABLE I. Chiral condensates on the $8^3\times 12$ lattice, region $\beta\sim\beta_{cd}$.

β	m_u	m_d	$\langle\overline{\chi_u}\chi_u\rangle$	$\langle\overline{\chi_d}\chi_d\rangle$
0.00	0.09	0.09	0.6312(11)	0.6323(11)
0.04	0.04	0.04	0.6346(17)	0.4036(13)
0.05	0.02	0.02	0.6302(23)	0.1881(15)
0.05	0.04	0.04	0.6295(17)	0.2515(10)
0.05	0.09	0.09	0.6258(11)	0.3339(8)
0.06	0.02	0.04	0.6180(24)	0.1392(6)
0.06	0.04	0.04	0.6243(17)	0.1397(5)
0.075	0.02	0.02	0.6067(23)	0.03988(10)
0.075	0.04	0.04	0.6073(16)	0.07898(22)
0.075	0.09	0.09	0.6061(11)	0.1662(3)
0.10	0.02	0.02	0.5569(22)	0.02602(4)
0.10	0.04	0.04	0.5640(16)	0.05380(9)
0.10	0.09	0.09	0.5664(10)	0.1148(1)
0.12	0.02	0.04	0.4970(19)	0.04357(5)

and two sets each with four flavors of staggered fermions which couple to the gauge fields with couplings 1 and $-1/2$, corresponding to u and d quarks with only electromagnetic interactions:

$$S_f=\sum_{x,y}\{\overline{\chi_u}(x)M_{u,xy}\chi_u(y)+\overline{\chi_d}(x)M_{d,xy}\chi_d(y)\}. \quad (3)$$

The coupling β is related to the bare electric charges e_k by $\beta=1/(c_k e_k)^2$, $k=1,2$. The lattice spacing a is set to 1. The fermion matrices are given by

$$M_{k,x,y}=D_{k,xy}+m_k\delta_{xy},$$

$$D_{k,xy}(x)=\frac{1}{2}\sum_{\mu}\eta_\mu(x)\{e^{c_k iA_\mu(x)}\delta_{y,x+\hat{\mu}}-e^{-c_k iA_\mu(y)}\delta_{y,x-\hat{\mu}}\}, \quad (4)$$

$$k=u,\ d;\quad c_u=1,\quad c_d=-1/2.$$

In the limit $m_d\to\infty$, this model goes over into noncompact QED with one charge [9,14]. For the gauge fields, periodic boundary conditions in all four directions were chosen, for the fermions, periodic spatial and antiperiodic temporal boundary conditions. The simulations were performed on lattices of size $8^3\times 12$. From simulations with one charge, one expects that for the chosen values of β, m_u, and m_d finite size effects are small [15]. For each simulated point (β,m_u,m_d) $\sim$1000 configurations in equilibrium were generated using a hybrid Monte Carlo algorithm. Every fifth was stored for spectrum and charge calculations.

Staggered fermions are a useful choice for studying chiral symmetry properties at finite lattice spacing. The action (3) of the two-charge model has for the kth species of fermions a chiral $U(1)_V\times U(1)_A$ symmetry, if $m_k=0$. The order parameters are the chiral condensates

$$\sigma_k\equiv\langle\overline{\chi_k}\chi_k\rangle=-\langle \mathrm{Tr}M_k^{-1}\rangle, \quad (5)$$

which are computed using a stochastic estimator [22]. Simulation results for the chiral condensates are shown in Tables I and II.

B. Determination of the critical points

In noncompact QED with one set of staggered fermions, the chiral condensate σ is consistent with an equation of state, similar to one arising from mean field theory but with logarithmic corrections, motivated from a linear σ model [15,23].

The parameters in the equation of state are expanded in a power series in the reduced coupling $(1-\beta/\beta_c)$, where β_c denotes the critical coupling. The logarithmic corrections are only expected to become important very close to the critical point because of renormalization effects. It is expected that also here they become relevant if one goes closer to the critical point. From the results in Tables I and II, and as illustrated for $\beta=0.18$ in Fig. 1, it appears that the chiral condensates are fairly independent of the other fermion's bare mass.

Thus to determine the critical points in the two-charge model, an ansatz with two uncoupled equations of state (similar to those arising from mean field theory but with logarithmic corrections) for both fermions is used:

$$m_k=2\tau_k\frac{\sigma_k}{\ln^{p_k}|\sigma_k^{-1}|}+4\theta_k\frac{\sigma_k^3}{\ln|\sigma_k^{-1}|},\quad k=u,d. \quad (6)$$

For the determination of the renormalization group flows it is desirable to know the chiral condensates as a function of (β,m_u,m_d) in the whole parameter space. It turns out to be possible to approximate the chiral condensates for all β with equations of state (6), using the following expansion of the couplings:

$$\tau_u/\theta_u=\tau_u^{(1)}(1-\beta/\beta_{cu})+\tau_u^{(3)}(1-\beta/\beta_{cu})^3,$$

$$1/\theta_u=\theta_u^{(0)}+\theta_u^{(1)}(1-\beta/\beta_{cu})+\theta_u^{(3)}(1-\beta/\beta_{cu})^3, \quad (7)$$

and

$$\tau_d/\theta_d=\tau_d^{(1)}(1-\beta/\beta_{cd}),$$

$$1/\theta_d=\theta_d^{(0)}+\theta_d^{(1)}(1-\beta/\beta_{cd}). \quad (8)$$

β_{ck}, $\tau_k^{(1,3)}$, $\theta_k^{(0,1,3)}$, and p_k are fit parameters. Including

TABLE II. Chiral condensates on the $8^3\times 12$ lattice, region $\beta\sim\beta_{cu}$.

β	m_u	m_d	$\langle\overline{\chi_u}\chi_u\rangle$	$\langle\overline{\chi_d}\chi_d\rangle$
0.14	0.02	0.02	0.4222(19)	0.01951(3)
0.15	0.02	0.02	0.3741(18)	0.01880(2)
0.15	0.04	0.04	0.4031(12)	0.03810(5)
0.15	0.09	0.09	0.4469(09)	0.08451(9)
0.16	0.02	0.02	0.3236(17)	0.01813(2)
0.16	0.02	0.04	0.3316(16)	0.03595(3)
0.16	0.04	0.02	0.3656(12)	0.01815(2)
0.16	0.04	0.04	0.3629(12)	0.03611(3)
0.16	0.09	0.09	0.4168(8)	0.08146(8)
0.17	0.02	0.02	0.2742(15)	0.01772(2)
0.17	0.04	0.04	0.3238(12)	0.03539(4)
0.17	0.09	0.09	0.3908(8)	0.07871(7)
0.18	0.02	0.02	0.2167(14)	0.01741(2)
0.18	0.02	0.04	0.2227(15)	0.03435(3)
0.18	0.02	0.09	0.2255(14)	0.07602(7)
0.18	0.04	0.02	0.2850(11)	0.01725(2)
0.18	0.04	0.04	0.2854(11)	0.03524(5)
0.18	0.04	0.09	0.2844(12)	0.07702(8)
0.18	0.09	0.02	0.3611(8)	0.01737(2)
0.18	0.09	0.04	0.3618(8)	0.03473(3)
0.18	0.09	0.09	0.3621(8)	0.07716(7)
0.19	0.02	0.02	0.1870(15)	0.01669(1)
0.19	0.04	0.04	0.2444(10)	0.03370(4)
0.19	0.09	0.09	0.3372(7)	0.07502(6)
0.20	0.02	0.02	0.1416(10)	0.01649(1)
0.20	0.02	0.16	0.1462(15)	0.1263(1)
0.20	0.04	0.04	0.2167(9)	0.03283(3)
0.20	0.09	0.09	0.3108(8)	0.07420(6)
0.20	0.16	0.02	0.3785(6)	0.01677(1)
0.21	0.02	0.02	0.1143(7)	0.01624(1)
0.21	0.02	0.16	0.1072(7)	0.1254(1)
0.21	0.04	0.04	0.1838(8)	0.03331(6)
0.21	0.09	0.09	0.2882(7)	0.07280(6)
0.21	0.16	0.02	0.3605(5)	0.01660(1)
0.22	0.04	0.04	0.1601(7)	0.03222(3)
0.22	0.09	0.09	0.2693(6)	0.07162(6)

all results for σ_u simulated at $m_u\leqslant 0.09$, one obtains $\beta_{cu}=0.173$. Values of the fit parameters and the fit errors are listed in Table III. For a fit of σ_d, all results with $\beta\leqslant 0.1$ and $m_d\leqslant 0.09$ have been used, and the critical coupling is $\beta_{cd}=0.047$. From varying the range of the chiral condensates included in the fit, one estimates the error on β_{cu} and β_{cd} to be approximately 0.001, which is larger than the fit error. Without including logarithmic corrections, β_{cu} comes out to be 0.183(1) and β_{cd} to be 0.049(1) [25]. The cubic term in Eq. (7) is included to obtain an approximate description of σ_u also in the region where $\beta\sim\beta_{cd}$. It has been checked that with a fit in the range $0.16\leqslant\beta\leqslant 0.22$, including only linear terms in the reduced coupling, one obtains the same result for β_{cu} within errors. As seen in Fig. 2, Eqs. (6) give a good description for the chiral condensates in the range of couplings $\beta\geqslant 0.05$. Two or three of the same symbols lying on top of each other at the β values 0.06, 0.16, 0.18, 0.20, and 0.21 correspond to simulations at various values of m_u at a fixed value of m_d or vice versa. One further notices that in the regions where the d fermion undergoes a transition, the u fermion is that far in the broken region that σ_u is practically independent of m_u (as well as of m_d).

C. Renormalized fermion masses

The next step in the investigation of the critical behavior is the determination of the renormalized fermion masses or inverse fermionic correlation lengths. Because the fermions are charged, their correlation functions are gauge dependent. For the calculation of their expectation value, a technique as described in Refs. [26,15] is used. First, the Landau gauge is fixed by imposing the gauge-fixing condition

$$\sum_\mu \overline{\Delta}_\mu A_\mu(x)=0, \tag{9}$$

where $\overline{\Delta}_\mu$ denotes the backward derivative on the lattice. An

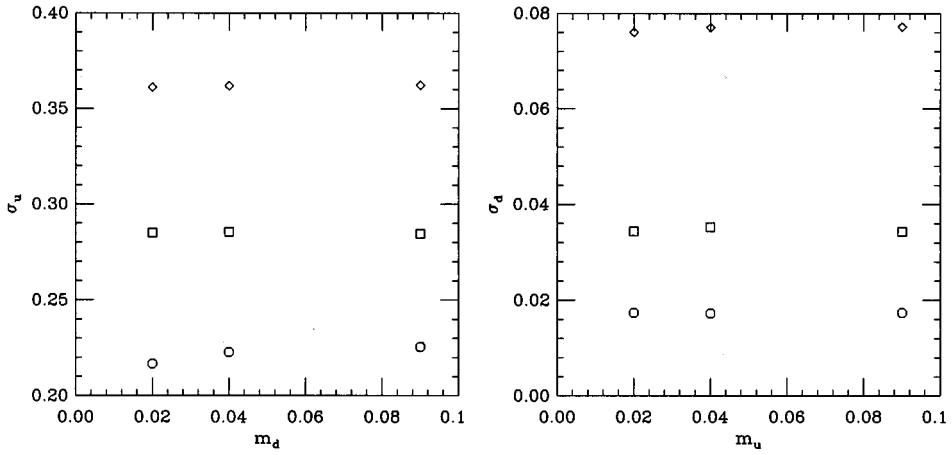

FIG. 1. Dependence of σ_u on $m \equiv m_d$ (left) and of σ_d on $m \equiv m_u$ (right). Circles denote $m = 0.02$, squares $m = 0.04$, and diamonds $m = 0.09$. $\beta = 0.18$. Statistical errors are smaller than the symbols.

additional gaugelike degree of freedom is the invariance of the action under the local transformation

$$A_\mu(x) \to A_\mu(x) + \Delta_\mu \alpha(x),$$
$$\chi(x) \to e^{-ic_k\alpha(x)}\chi_k(x),$$
$$\overline{\chi_k}(x) \to e^{ic_k\alpha(x)}\overline{\chi_k}(x), \tag{10}$$

with

$$\alpha(x) = \sum_\mu \frac{4\pi}{L_\mu} n_\mu x_\mu, \quad n_\mu \in \mathbb{Z}. \tag{11}$$

The lattice average of the gauge field

$$\overline{A_\mu} = \frac{1}{V}\sum_x A_\mu(x), \quad V = \prod_\mu L_\mu, \tag{12}$$

has a nonvanishing expectation value on our (relatively small) ensembles. By shifting it by multiples of $4\pi/L_\mu$, such that it is restricted to the interval $(-2\pi/L_\mu, 2\pi/L_\mu]$, this additional degree of freedom was fixed. In the two-charge model, this interval is chosen twice as large as in a model with fermions of charge 1. This is necessary to preserve also the boundary conditions of the d fermion, which couples with charge $-1/2$. $\overline{A_\mu}$ is approximately constant over $\sim$10–20 configurations. Following the procedure described in [26,15], the set of data samples at each parameter value was divided into subsets of 10–20. The correlation functions were averaged over each subset and fitted with the free form of a staggered fermion propagator in a constant background field B_μ. For the u fermion, B_μ agrees with the expectation value of $\overline{A_\mu}$, taken over the given subset, for the d fermion with the expectation value of $-\overline{A_\mu}/2$. The fits were performed with the routine MINUIT. The ansatz gives a good description of the data. An example for this is shown in Fig. 4. Results are given in Tables IV and V. Another indication that the fermion correlation functions behave similar to free propagators with a renormalized mass $m_{u,dR}$, is obtained by comparing the simulation data for the chiral condensates with free propagator expressions:

$$\langle \overline{\chi_k}\chi_k \rangle = \frac{1}{V}\sum_{p_\mu} \frac{m_{kR}}{\Sigma_\mu \sin^2 p_\mu + m_{kR}^2}, \quad k = u,d, \tag{13}$$

with the lattice momenta

$$p_i = \frac{2\pi}{L_i} n_i, \quad n_i = 1, \ldots, L_i, \quad i = 1, \ldots, 3$$

TABLE III. Fit parameters for the equation of state with logarithmic corrections.

β_{cu}	0.1729(2)	β_{cd}	0.04675(7)
$\tau_u^{(1)}$	−1.78(1)	$\tau_d^{(1)}$	−1.469(9)
$\tau_u^{(3)}$	0.48(3)		
$\theta_u^{(0)}$	2.61(2)	$\theta_d^{(0)}$	2.41(2)
$\theta_u^{(1)}$	−1.3(1)	$\theta_d^{(1)}$	−1.42(2)
$\theta_u^{(3)}$	−5.7(6)		
p_u	0.588(6)	p_d	0.074(3)

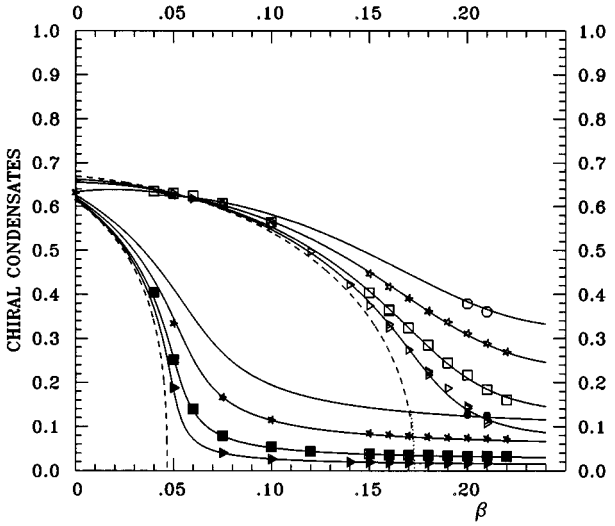

FIG. 2. Chiral condensates (open symbols: σ_u^β, filled symbols: σ_d) as a function of β with a mean-field fit with logarithmic corrections. Triangles correspond to $m_k = 0.02$, squares to $m_k = 0.04$, asterisks to $m_k = 0.09$, and circles to $m_k = 0.16$, $k = u,d$. The solid lines show the result of the fits and the dashed lines solutions of the equations of state with m_k set to 0.

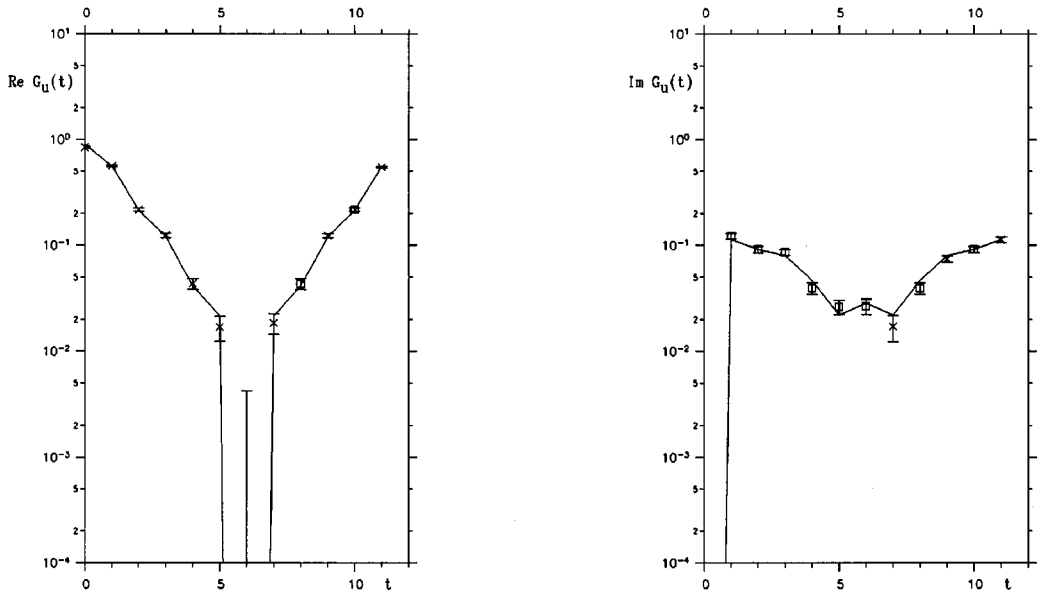

FIG. 3. u fermion propagators at $\beta=0.16$ and $m_u=m_d=0.02$. Crosses correspond to positive values of the correlation function, squares to negative values. Solid lines denote the fit.

$$p_4=\frac{\pi}{L_4}(2n_4-1), \quad n_4=1,\ldots,L_4.$$

Figures 5 and 6 show that for small masses the results agree quite well with Eqs. (13). The fermion wave function renormalization constant is of order 1. Since $m_{kR}\propto\langle\overline{\chi}_k\chi_k\rangle$ for small m_{kR}, Eqs. (6) and (7) imply that near $\beta\simeq\beta_{cu}$ the renormalized u mass scales according to

$$m_{uR}\ln^{-1/3}(m_{uR}^{-1})\propto m_u^{1/3}, \tag{14}$$

and the renormalized d mass according to

$$m_{dR}\ln^{-p_d}(m_{dR}^{-1})\propto m_d. \tag{15}$$

The scaling behavior of the d is thus in this region close to the perturbative behavior, which is very different from the behavior of the u fermion in this region. For very large β, both renormalized masses follow Eq. (15). In the neighborhood of $\beta\simeq\beta_{cd}$, Eqs. (6) and (7) indicate that

$$m_{dR}\ln^{-1/3}(m_{dR}^{-1})\propto m_d^{1/3}. \tag{16}$$

In this region the difference between the bare and renormalized masses of the d becomes small.

D. Phase diagram

Figure 7 shows a sketch of the phase diagram. The agreement of the results with Eq. (6) suggests that there are two

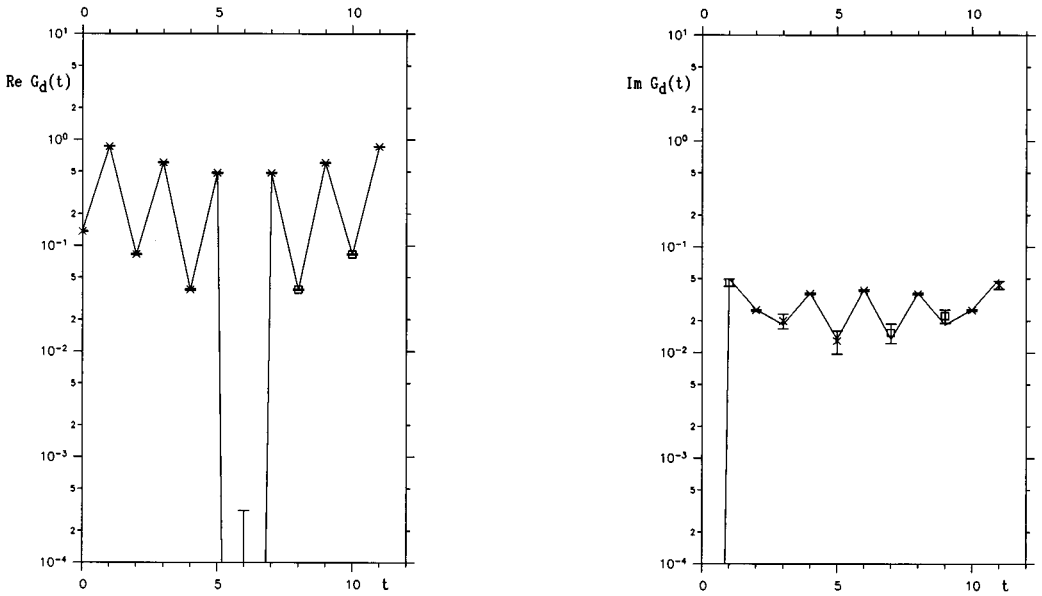

FIG. 4. d fermion propagators at $\beta=0.16$ and $m_u=m_d=0.02$. The meaning of the symbols is explained in the caption of the previous figure.

TABLE IV. Renormalized fermion masses and coupling, region $\beta \sim \beta_{cd}$.

β	m_u	m_d	m_{uR}	m_{dR}	β_R
0.05	0.02	0.02	5.000(675)	0.326(7)	0.073(1)
0.05	0.04	0.04	4.935(143)	0.446(4)	0.069(1)
0.05	0.09	0.09	5.646(604)	0.644(7)	0.063(1)
0.06	0.02	0.04	2.872(393)	0.258(4)	0.087(1)
0.06	0.04	0.04	2.573(382)	0.252(3)	0.088(1)
0.075	0.02	0.02	2.018(143)	0.085(1)	0.123(1)
0.075	0.04	0.04	1.993(210)	0.149(2)	0.116(1)
0.075	0.09	0.09	2.912(126)	0.295(2)	0.104(1)
0.10	0.02	0.02	1.518(074)	0.050(1)	0.163(2)
0.10	0.04	0.04	1.864(120)	0.090(1)	0.154(1)
0.10	0.09	0.09	1.662(92)	0.209(2)	0.139(1)
0.12	0.02	0.04	1.124(37)	0.072(1)	

TABLE V. Renormalized fermion masses and coupling, region $\beta \sim \beta_{cu}$.

β	m_u	m_d	m_{uR}	m_{dR}	β_R
0.14	0.02	0.02	0.917(28)	0.034(1)	0.238(3)
0.15	0.02	0.02	0.753(13)	0.032(1)	0.257(2)
0.15	0.04	0.04	0.858(9)	0.065(1)	0.239(2)
0.15	0.09	0.09	1.023(13)	0.148(1)	0.215(2)
0.16	0.02	0.02	0.609(7)	0.031(1)	0.276(3)
0.16	0.02	0.04	0.617(8)	0.063(1)	0.264(3)
0.16	0.04	0.02	0.727(9)	0.033(1)	0.272(2)
0.16	0.04	0.04	0.714(10)	0.064(1)	0.258(2)
0.16	0.09	0.09	0.918(9)	0.143(1)	0.232(2)
0.17	0.02	0.02	0.485(7)	0.030(1)	0.304(3)
0.17	0.04	0.04	0.607(8)	0.061(1)	0.274(3)
0.17	0.09	0.09	0.815(5)	0.139(1)	0.250(2)
0.18	0.02	0.02	0.366(7)	0.029(1)	0.329(3)
0.18	0.02	0.04	0.384(5)	0.058(1)	0.321(3)
0.18	0.02	0.09	0.379(4)	0.130(1)	0.305(3)
0.18	0.04	0.02	0.506(5)	0.029(1)	0.315(3)
0.18	0.04	0.04	0.512(6)	0.058(1)	0.303(3)
0.18	0.04	0.09	0.512(5)	0.130(1)	0.288(3)
0.18	0.09	0.02	0.720(4)	0.030(1)	0.291(2)
0.18	0.09	0.04	0.715(4)	0.060(1)	0.278(2)
0.18	0.09	0.09	0.720(6)	0.133(1)	0.268(2)
0.19	0.02	0.02	0.319(6)	0.029(1)	0.357(3)
0.19	0.04	0.04	0.425(4)	0.057(1)	0.321(3)
0.19	0.09	0.09	0.658(4)	0.134(1)	0.279(2)
0.20	0.02	0.02	0.229(7)	0.028(1)	0.388(3)
0.20	0.02	0.16	0.245(4)	0.219(1)	0.351(3)
0.20	0.04	0.04	0.372(5)	0.056(1)	0.342(3)
0.20	0.09	0.09	0.596(6)	0.128(1)	0.299(2)
0.20	0.16	0.02	0.807(6)	0.030(1)	0.303(2)
0.21	0.02	0.02	0.182(4)	0.027(1)	0.415(2)
0.21	0.02	0.16	0.171(2)	0.213(1)	0.351(3)
0.21	0.04	0.04	0.311(3)	0.055(1)	0.367(3)
0.21	0.09	0.09	0.528(5)	0.125(1)	0.315(2)
0.21	0.16	0.02	0.735(7)	0.029(1)	0.318(2)
0.22	0.04	0.04	0.268(4)	0.054(1)	0.386(3)
0.22	0.09	0.09	0.491(3)	0.124(1)	0.328(2)

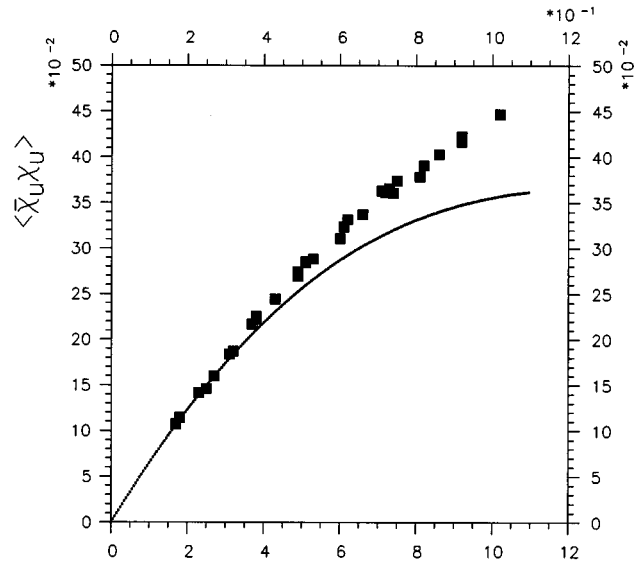

FIG. 5. Chiral condensate $\langle\overline{\chi_u}\chi_u\rangle$ for $\beta\geqslant 0.14$ plotted against the renormalized mass m_{uR}. The line denotes Eq. (13).

distinct regions of chiral symmetry breaking for both fermion species. This does not correspond to the expectations in a confining theory. If chiral symmetry breaking in noncompact QED was related to confinement, one would expect both species of fermions to develop chiral condensates in the same time. The end points of the phase boundary of the u, which separates the symmetric phase of the u on the $m_u=0$ surface from its broken phase, are given by β_{cu} and β_c, the critical point of QED with one set of u fermions [15] which is the limit of the two-charge model if $m_d\to\infty$. In the presence of more charges, the critical point is shifted towards stronger coupling, so β_{cu} is slightly smaller than β_c. In the limit $m_u\to\infty$, which corresponds to QED with one set of charges with coupling $\beta=4/e^2$, one expects this to occur at

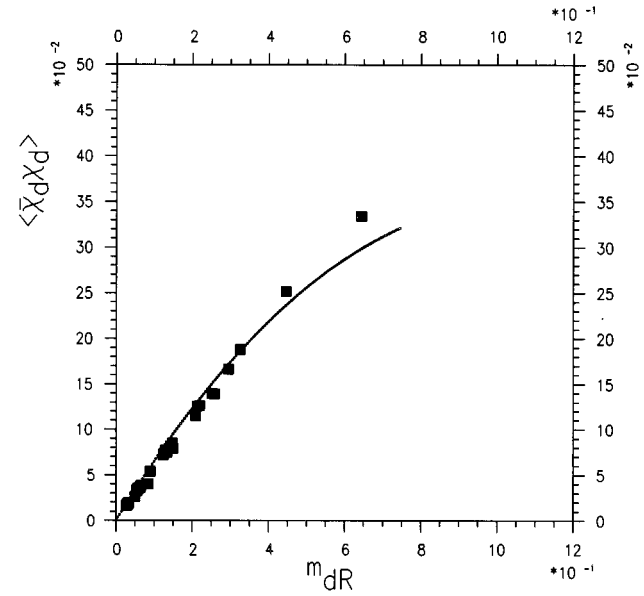

FIG. 6. Chiral condensate $\langle\overline{\chi_d}\chi_d\rangle$ plotted against m_{dR}. The line denotes Eq. (13).

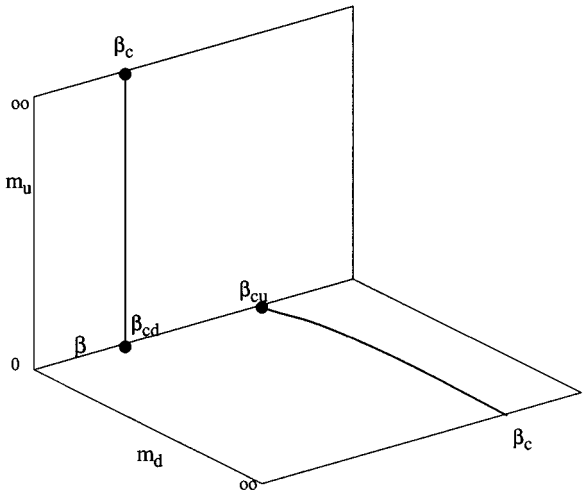

FIG. 7. Sketch of the phase diagram.

$\beta_c/4$ (~ 0.046, using the result of [15]). In the two-charge model, a value very close to this is obtained, $\beta_{cd}\simeq 0.047$. Below β_{cu}, no continuum limit with two fermion species is possible. For the investigated parameter values at $\beta\leqslant 0.14$, the renormalized u masses are of order 1 in lattice units, which means the u fermion is, in this parameter region, essentially not present in the spectrum. In the region $\beta\gtrsim\beta_{cu}$, both fermion masses can go to zero, so this region is the most interesting candidate for a continuum limit of the model.

III. THE RENORMALIZED COUPLING

A. Charge determination on the lattice

The Ward identities ensure that the charge renormalization is entirely determined by the wave function renormalization of the photon:

$$e^2_{u,dR}=Z_3 e^2_{u,d}. \tag{17}$$

Z_3 is given by the zero-momentum limit of the gauge-invariant part of the photon propagator:

$$D(k)=\frac{\beta}{N_k V}\sum_{\mu,k|\hat{k}^2=\text{const},\ k_\mu=0}\hat{k}^2\langle\tilde{A}_\mu(\hat{k})\tilde{A}_\mu(-\hat{k})\rangle\,|_{k_\mu=0}, \tag{18}$$

$$Z_3=\lim_{k\to 0}D(k). \tag{19}$$

The sum in Eq. (18) runs over all directions μ and for each μ over all N_k choices of k with fixed k^2 and $k_\mu=0$. Because of the lattice, the momenta enter the photon propagator as

$$\hat{k}_\mu=e^{ik_\mu}-1 \quad\text{and}\quad \hat{k}^2=\hat{k}_\mu\hat{k}^*_\mu. \tag{20}$$

The right-hand side (RHS) of (18) turns out to be strongly fluctuating and inappropriate for an extrapolation to $k\to 0$. Thus for the calculation of $D(k)$, a method analogous to Refs. [14,15,27] is used. The photon propagator $D(k)$ is re-expressed using the Ward identities [28] in terms of a correlator between the gauge field and the fermion current:

$$D(k)=1-\frac{1}{N_k V}\sum\langle\tilde{j}_\mu(\hat{k})\tilde{A}_\mu(-\hat{k})\rangle\,\Big|_{k_\mu=0}, \tag{21}$$

where in the two-charge model

$$j_\mu(x)=\frac{\delta}{\delta A_\mu(x)}\sum_{yz}\{\overline{\chi_u}(y)M_{u,yz}\chi_u(z)+\overline{\chi_d}(y)M_{d,yz}\chi_d(z)\}. \tag{22}$$

The correlator in Eq. (21) has less fluctuations and could be used for an extrapolation of $D(k)$ to $k\to 0$. The fermion current was computed using a stochastic estimator with 30–75 inversions of the fermion matrices.

B. Comparison with perturbation theory

Taking contributions of both fermions into account, in one-loop perturbation theory the vacuum polarization tensor has the form

$$1/\beta\Pi_{\mu\nu}(k,m_{uR},m_{dR},V)=e_u^2\Pi^{(1)}_{\mu\nu}(k,m_{uR},V)+e_d^2\Pi^{(1)}_{\mu\nu}(k,m_{dR},V), \tag{23}$$

where $\Pi^{(1)}_{\mu\nu}(k,m_R,V)$ is the vacuum polarization tensor for a single set of fermions with the renormalized mass m_R on a lattice of volume V. Projection onto the gauge-invariant part yields

$$D(k)=1+e_u^2\Pi^{(1)}(k,m_{uR},V)+e_d^2\Pi^{(1)}(k,m_{dR},V), \tag{24}$$

where $\Pi^{(1)}(k,m_R,V)$ is the one-loop vacuum polarization function for one set of staggered fermions:

$$\Pi^{(1)}(k,m_R,V)=\frac{1}{\hat{k}^2}[\Pi^{(1)}_{\mu\mu}(k,m_R,V)-\Pi^{(1)}_{\mu\mu}(0,m_R,V)]|_{k_\mu=0}. \tag{25}$$

The second term on the right-hand side occurs because $\Pi^{(1)}_{\mu\mu}(0,m_R,V)\neq 0$ for a finite V. This would correspond to a finite photon mass, and the term is subtracted. Here, a fixed μ has been chosen with $k_\mu=0$. Finally, one obtains, for the photon propagator in the two-charge model,

$$\frac{\beta}{D(k)}=\beta_R+\Pi(0,m_{uR},m_{dR},\infty)-\Pi(k,m_{uR},m_{dR},V). \tag{26}$$

Extrapolating this to $V\to\infty,\quad k\to 0$,

$$\beta_R=\beta-\Pi(0,m_{uR},m_{dR},\infty) \tag{27}$$

gives the perturbative relation between the bare and the renormalized coupling. Combining the last two expressions, one gets the fit formula for the Monte Carlo results for $D(k)$:

$$\frac{\beta}{D(k)}=\beta_R+\Pi(0,m_{uR},m_{dR},\infty)-\Pi(k,m_{uR},m_{dR},V). \tag{28}$$

The renormalized coupling β_R is the only free parameter in the fit.

For the calculation of $\Pi(0,m_{uR},m_{dR},\infty)$, the effect of the zero modes $\overline{A_\mu}$ of the gauge field has to be taken into account. Their contribution is important where fermions are light, as are the d fermions at the simulated parameter values with $\beta\sim\beta_{cu}$. To calculate the perturbative vacuum polarization functions, the background fields are integrated over:

$$\Pi(k,m_{uR},m_{dR},V)=\frac{\int d^4\overline{A}\det(D_u+m_u)\det(D_d+m_d)\sum_p\rho(p,k,\overline{A},m_{uR},m_{dR},V)}{\int d^4\overline{A}\det(D_u+m_u)\det(D_d+m_d)}. \tag{29}$$

Also, in the presence of constant background fields the fermion determinant of free fermions can be written as a product of contributions with definite momentum:

$$\det M_i=\det(D_i+m_i)=\prod_{k_i}\left[m_i^2+\sum_\mu\sin^2(k_{i,\mu}+c_i\overline{A_\mu})\right]^{1/2},\quad i=u,d, \tag{30}$$

with $c_u=1$ and $c_d=-1/2$. Choosing $\mu=3$ in Eq. (25), the function ρ looks as

$$\rho=\sum_{i=u,d}\left[-2\frac{\sum_{\mu\neq 3}[\cos(\tilde{k}_{i,\mu})\sin(p_\mu/2)]^2}{D(\tilde{k}_i-p,m_{iR})D(\tilde{k}_i+p,m_{iR})}+\sin^2[(\tilde{k}_{i,3}-p_3)/2]\left\{\frac{1}{D(\tilde{k}_i-p,m_{iR})}-\frac{1}{D(\tilde{k}_i+p,m_{iR})}\right\}^2\right]\cos^2(\tilde{k}_{i,3}), \tag{31}$$

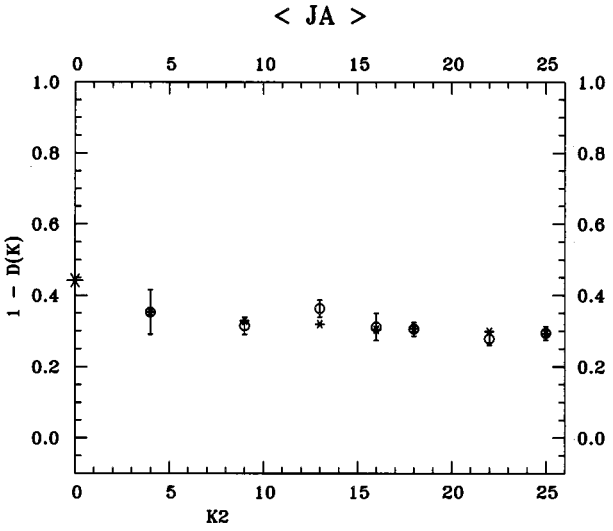

FIG. 8. Photon propagator $\beta = 0.17$, $m_u = m_d = 0.02$. The circles describe the data and the asterisks the fit with the perturbative formula. The extrapolation to $k \to 0$ is denoted by an asterisk. The variable $K2$ on the x axis is defined as $K2 = 576/(2\pi)^2 k^2$ to be an integer.

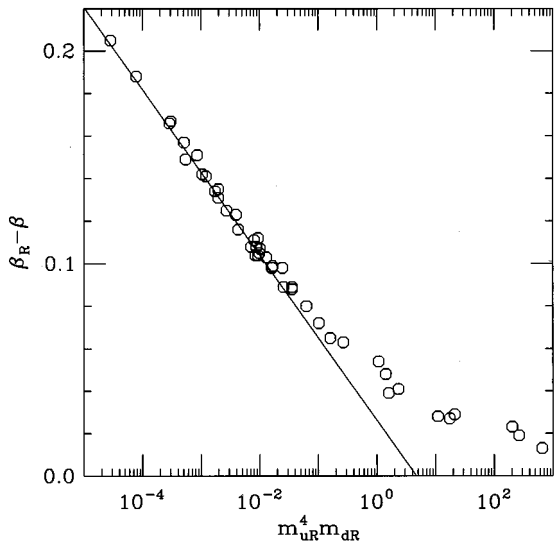

FIG. 9. Renormalized couplings in the region of small m_{uR} and m_{dR}. The line denotes the small mass limit of one-loop perturbation theory.

where

$$D(k,m_R) = m_R^2 + \sum_\mu \sin^2(k_\mu/2) \tag{32}$$

and

$$\tilde{k}_u = k_u + \overline{A} \quad \text{and} \quad \tilde{k}_d = k_d - \overline{A}/2. \tag{33}$$

The integral over the background fields was evaluated using a Monte Carlo method, representing the background fields through Gaussian random numbers and calculating the weight of the fermion determinant in the presence of these background fields. Figure 8 shows an example for a fit of $D(k)$ with one-loop perturbation theory in the presence of background fields. The oscillations of $D(k)$ are caused by the dependence of k on the direction because of the asymmetry of the lattice. The renormalized couplings are listed in Tables IV and V.

The renormalized coupling can be calculated directly in perturbation theory using Eq. (27). One would like to compare the data with the perturbative result. Since this is of interest especially in regions of a high cutoff, i.e. for small masses, the limit $m_{uR}, m_{dR} \ll 1$ of the vacuum polarization function (27) is taken, which gives

$$\beta_R - \beta = -\Pi(0, m_{uR}, m_{dR}, \infty) = -\frac{1}{6\pi^2} \ln(m_{uR}^4 m_{dR}) + 5c/4. \tag{34}$$

From QED with one species of fermions with charge 1, it is known that $c \simeq 0.0210$ [15]. Figure 9 shows that in the small mass limit the renormalized charges indeed follow the logarithmic behavior as in the right-hand side of Eq. (34). For larger masses, Π is no more a function of $m_{uR}^4 m_{dR}$ alone, but the simulation results are still in agreement with perturbation theory [30]. There does not seem to be any effect on charge renormalization from possible charged bound states.

The agreement with perturbation theory indicates that this model is trivial in the limit of infinite cutoff, and that all renormalized charges vanish if only one fermion mass goes to zero. The renormalized coupling vanishes in those parts of the phase diagram (see Fig. 7) where σ_u or σ_d equal zero.

One would now like to find a relation between a finite renormalized coupling and a corresponding cutoff. The ratio of the renormalized masses has to be kept constant while the cutoff is varied. Reexpressing (34) in terms of $R = m_{uR}/m_{dR}$ and exponentiating, one obtains

$$m_{uR} = 1.365 R^{1/5} \exp\left(-\left[\frac{6\pi^2}{5} (\beta_R - \beta) \right] \right). \tag{35}$$

From this equation one will be able to estimate the maximal cutoff belonging to each renormalized charge. For this, one needs to know which β coordinate the point with maximal cutoff on a renormalization group flow line with fixed β_R and R has. This flow line will be the intersection between the surface with fixed R and the one with fixed β_R in the three-dimensional parameter space.

C. Renormalization group flow of the coupling

It is not feasible to cover all the regions of the phase diagram that are of interest with simulations. For a determination of the renormalization group flows of the charge, one therefore has to make use of extrapolation methods. If one is able to find a functional dependence of the renormalized mass on the bare parameters, it is possible to calculate the renormalized coupling using perturbation theory from Eq. (27). The chiral condensates can be approximated as functions of β, m_u, and m_d through the equations of state. Figures 5 and 6 suggest that the renormalized masses can be expressed as functions of the chiral condensate, where for small masses there is agreement with the free propagator relation Eq. (13), and the leading term is linear. For the

TABLE VI. Fit parameters for the renormalized fermion masses.

P_1	1.54(1)	Q_1	1.726(3)
P_2	3.5(1)	Q_2	

renormalization group flows, one is primarily interested in regions where both fermion masses are smaller than 1, so m_{uR} is fitted for $\beta \geq 0.14$ with the ansatz

$$m_{uR} = P_1 \langle \overline{\chi_u} \chi_u \rangle + P_2 \langle \overline{\chi_u} \chi_u \rangle^3. \tag{36}$$

Here, χ^2 per degree of freedom is 1.5. The following fit gives a good description for the d mass for $\beta \geq 0.14$:

$$m_{dR} = Q_1 \langle \overline{\chi_d} \chi_d \rangle, \tag{37}$$

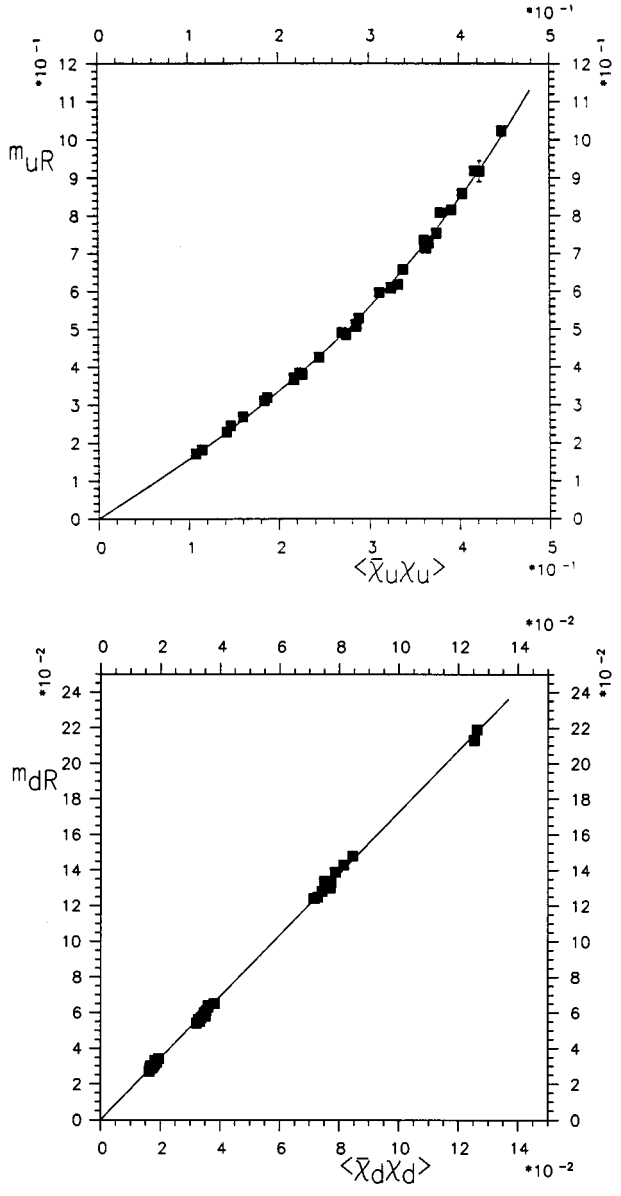

FIG. 10. Renormalized masses as a function of the chiral condensates. The squares denote simulation results and lines the fit according to Eqs. (36) and (37), respectively.

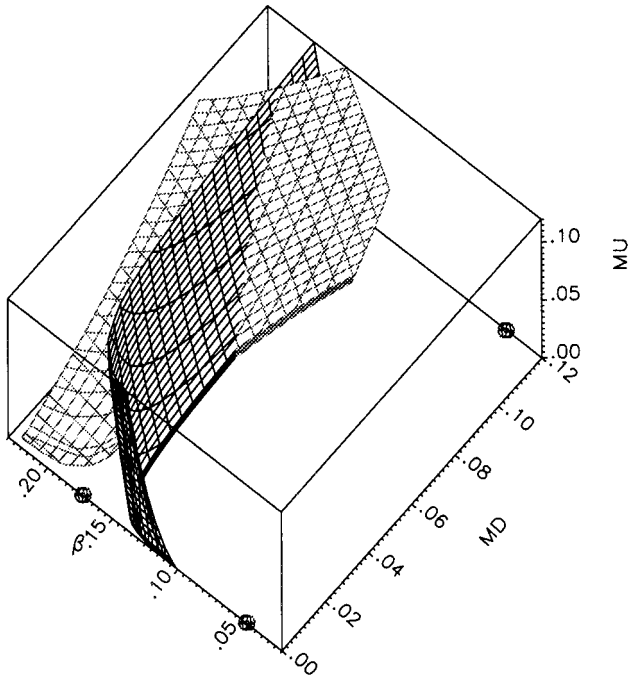

FIG. 11. Surfaces with $\beta_R = 0.27$ (black) and $R = 5$ (grey). The little spheres denote β_{cu} and β_{cd}.

with χ^2 per degree of freedom equal to 2.2. A cubic term is not needed here. The fit parameters P and Q are given in Table VI. As illustrated in Fig. 10, one thus obtains a good description for the renormalized masses.

To obtain the renormalized masses as a function of the bare parameters, first the equations of state were solved explicitly for the chiral condensates using Müller's method [31] for calculating zeros of nonlinear functions. The results were thus inserted into the fit equations (36) and (37), respectively.

Using this method, a grid of values for the mass ratio R in the phase diagram is generated and, using renormalized perturbation theory, also for β_R. Using a graphics package, surfaces of constant β_R and R can be drawn. Figure 11 shows a surface S_{β_R} (black) with a constant β_R and its intersection with a surface S_R (grey) of constant R of $O(1)$.

For large m_u and m_d, both renormalized fermion masses are large. Therefore, $\beta_R \sim \beta$ which implies that surfaces with fixed β_R are nearly perpendicular to the β axis. The behavior at small m_u, m_d can be read off from Eq. (34). If m_u is lowered, the surfaces bend over until they end on the $m_u = 0$ plane below the line where the chiral symmetry of the u fermion is broken. The larger β_R is, the closer the end line of the surface on the $m_u = 0$ plane comes to the critical line of the u, except for very small m_d. In a whole range of $\beta < \beta_{cu}$ and small bare masses, m_{dR} is much smaller than m_{uR} and for constant m_d nearly constant. So, surfaces with constant β_R bend at small m_d towards small β, as the black surface in Fig. 11 indicates. They intersect the $m_d = 0$ plane in the broken phase of the d fermion, and thus cut the β axis at $\beta < \beta_{cd}$. The important point to note is that S_{β_R} intersects the surfaces $m_u = 0$ or $m_d = 0$ only in regions where both renormalized fermion masses are nonzero.

Surfaces of constant R end for $\beta \geq \beta_{cu}$ on the β axis. The

TABLE VII. Sign factors for the meson operators. The σ particle is provided with a hat to avoid confusion with the chiral condensates introduced earlier.

i	$s_i(\vec{x},t)$	Quantum numbers	Continuum states
1	$(-1)^t$	0_s^{++}	$\hat{\sigma}$
		0_a^{-+}	π'
2	$(-1)^{x_1+x_2+x_3+t}$	0_a^{+-}	$-$
		0_a^{-+}	π

scaling behavior of the masses in Eqs. (14) and (15) implies that at $\beta=\beta_{cu}$, these surfaces obey the relation $m_u \sim c m_d^3$, where c is a constant. If β is lowered past β_{cu}, m_{uR} increases quickly. As indicated in Fig. 11, the end line of the surfaces with constant R on the $m_u=0$ plane therefore has to turn away from the β axis and stay at a finite value of m_d. For an estimate of the validity bound, the intersection line of both surfaces is of interest, as it represents a flow line where both R and β_R are constant while the cutoff scale is changed. It ends on the $m_u=0$ plane at $\beta<\beta_{cu}$. As one moves down along the intersection line, the cutoff becomes larger, but never reaches infinity.

D. Validity bound

In noncompact QED with four flavors of staggered fermions of charge 1, the β function goes, in the limit of small renormalized mass, over into the prediction of one-loop continuum perturbation theory for four fermion flavors of charge 1 [15]. In the two-charge model with four flavors of charge 1 and four flavors of charge $-1/2$, a corresponding relation is satisfied (34). This suggests that in the presence of N species of fermions, the renormalized charge can be approximated with the formula

$$\beta_R-\beta=-\sum_{i=1}^{N}\frac{Q_i^2}{6\pi^2}\ln(am_{iR})+\sum_{i=1}^{N}Q_i^2 c. \tag{38}$$

In this section the lattice spacing a is kept explicitly, to illustrate the dependence on the cutoff. In QED with one charge and in the two-charge model, it was reasonable to approximate the bare charge corresponding to the point of maximal cutoff by the critical coupling of the fermion with the strongest coupling. This critical coupling is dependent on the number of dynamical fermions. Comparing β_c, determined using mean field equations of state or mean field equations of state with logarithmic corrections, in the quenched case, in models with four flavors of charge 1 [15], with eight flavors of charge 1 [32] and the two-charge model, one finds the behavior

$$\beta_c(N\text{species})=\beta_c(\text{quenched})-\epsilon\sum_{i=1}^{N}Q_i^2, \tag{39}$$

where $\epsilon\simeq 0.01$.

In the standard model, one has three generations of fermions of charge 1, three generations and colors of charge 2/3, and three generations and colors of charge 1/3. Expressing the electron mass in units of the cutoff and the other fermion masses in terms of ratios with the electron mass, one obtains

$$am_{eR}\gtrsim 3.68\exp\left\{-\frac{3\pi^2}{4}\beta_R\right\}\times(R_\mu R_\tau)^{1/8}(R_u R_c R_t)^{1/6}(R_d R_s R_b)^{1/24}, \tag{40}$$

where $R_\mu=m_{eR}/m_{\mu R}$, etc. The relation between the lattice spacing a and the cutoff Λ is approximately given by the relation

$$\Lambda\simeq 1/a. \tag{41}$$

Using the physical fermion masses and the physical value of the fine structure constant 1/137, one gets the cutoff

$$\Lambda\lesssim 10^{32}\ \text{GeV}. \tag{42}$$

This is much larger than the Planck scale (10^{19} GeV). However, if there are more charged particles, e.g., because of supersymmetry, the exponential dependence on the number of charged particles might cause this cutoff to become considerably lower.

If, on the other hand, one sets the validity bound of QED to be at the Planck scale, one obtains the upper bound on the fine structure constant

$$\alpha_R\lesssim 1/80, \tag{43}$$

which is surprisingly small. One also has to note that in Eq. (43), the effect of charged $W^{\pm}$ bosons is not yet included.

IV. COMPOSITE STATES

A. Lattice operators and fits

Correlation functions of scalar and pseudoscalar $\overline{uu}$ and $\overline{dd}$ states were investigated:

$$C_{u,i}(t)=\left\langle\sum_{\vec{x}} s_i(\vec{x},t)\overline{\chi_u}(\vec{x},t)\chi_u(\vec{x},t)\overline{\chi_u}(0)\chi_u(0)\right\rangle, \quad i=1,2, \tag{44}$$

$$C_{d,i}(t)=\left\langle\sum_{\vec{x}} s_i(\vec{x},t)\overline{\chi_d}(\vec{x},t)\chi_d(\vec{x},t)\overline{\chi_d}(0)\chi_d(0)\right\rangle, \quad i=1,2. \tag{45}$$

The sign factors s_i determine the lattice representation a state belongs to [34]. The corresponding continuum quantum numbers and states in QCD terminology are listed in Table VII. To reduce statistical fluctuations, for each correlation

TABLE VIII. Energies of neutral composite states, region $\beta \sim \beta_{cd}$.

β	m_u	m_d	m_{π_u}	m_{π_d}	m_{σ_d}
0.05	0.02	0.02	0.305(1)	0.431(1)	0.714(12)
0.05	0.04	0.04	0.431(0)	0.556(1)	0.950(21)
0.05	0.09	0.09	0.648(0)	0.783(1)	1.219(16)
0.06	0.02	0.04	0.307(1)	0.694(2)	0.798(3)
0.06	0.04	0.04	0.433(1)	0.695(2)	0.794(3)
0.075	0.02	0.02	0.311(1)	0.937(2)	0.934(2)
0.075	0.04	0.04	0.438(1)	0.933(2)	0.941(2)
0.075	0.09	0.09	0.657(0)	0.965(1)	1.045(2)
0.10	0.02	0.02	0.319(1)	1.124(3)	1.126(3)
0.10	0.04	0.04	0.450(1)	1.042(3)	1.052(3)
0.10	0.09	0.09	0.671(1)	1.142(3)	1.173(3)

TABLE IX. Energies of neutral composite states, region $\beta \sim \beta_{cu}$.

β	m_u	m_d	m_{π_u}	m_{π_d}	m_{σ_u}	m_{σ_d}
0.15	0.02	0.02	0.361(1)	1.229(2)	0.822(130)	1.229(2)
0.15	0.04	0.04	0.502(1)	1.189(2)	1.216(99)	1.191(2)
0.15	0.09	0.09	0.723(1)	1.241(2)	1.332(94)	1.255(2)
0.16	0.02	0.02	0.381(1)	1.239(2)	0.847(53)	1.240(2)
0.16	0.02	0.04	0.379(1)	1.261(2)	0.769(52)	1.262(2)
0.16	0.04	0.02	0.515(1)	1.264(2)	1.161(68)	1.264(2)
0.16	0.04	0.04	0.514(1)	1.274(2)	1.083(55)	1.275(2)
0.16	0.09	0.09	0.737(1)	1.267(2)	1.320(55)	1.279(2)
0.17	0.02	0.02	0.407(1)	1.217(2)	0.881(33)	1.217(2)
0.17	0.04	0.04	0.539(1)	1.243(2)	1.010(33)	1.244(2)
0.17	0.09	0.09	0.752(1)	1.307(2)	1.266(36)	1.318(2)
0.18	0.02	0.02	0.444(1)	1.192(2)	0.774(15)	1.193(2)
0.18	0.02	0.04	0.431(1)	1.242(2)	0.762(15)	1.243(2)
0.18	0.02	0.09	0.436(1)	1.280(2)	0.755(14)	1.287(2)
0.18	0.04	0.02	0.558(1)	1.274(2)	1.003(19)	1.274(2)
0.18	0.04	0.04	0.563(1)	1.188(3)	0.958(17)	1.184(3)
0.18	0.04	0.09	0.563(1)	1.241(2)	0.946(16)	1.254(2)
0.18	0.09	0.02	0.767(1)	1.283(2)	1.266(24)	1.277(2)
0.18	0.09	0.04	0.768(1)	1.276(2)	1.252(23)	1.284(2)
0.18	0.09	0.09	0.769(1)	1.282(2)	1.256(23)	1.293(2)
0.19	0.02	0.02	0.444(1)	1.305(2)	0.734(11)	1.305(2)
0.19	0.04	0.04	0.588(1)	1.262(2)	0.903(9)	1.260(2)
0.19	0.09	0.09	0.776(1)	1.327(2)	1.246(18)	1.334(2)
0.20	0.02	0.02	0.509(2)	1.282(2)	0.655(4)	1.281(2)
0.20	0.02	0.16	0.496(2)	1.357(2)	0.647(5)	1.390(2)
0.20	0.04	0.04	0.600(1)	1.306(2)	0.856(73)	1.307(2)
0.20	0.09	0.09	0.802(1)	1.294(2)	1.159(10)	1.302(2)
0.20	0.16	0.02	0.995(1)	1.314(2)	1.432(17)	1.314(2)
0.21	0.02	0.02	0.579(2)	1.271(2)	0.659(2)	1.271(2)
0.21	0.02	0.16	0.592(2)	1.317(2)	0.667(3)	1.366(2)
0.21	0.04	0.04	0.645(1)	1.212(3)	0.824(4)	1.205(3)
0.21	0.09	0.09	0.806(1)	1.326(2)	1.154(9)	1.332(2)
0.21	0.16	0.02	1.009(1)	1.285(2)	1.395(13)	1.286(2)
0.22	0.04	0.04	0.679(2)	1.282(2)	0.817(4)	1.281(2)
0.22	0.09	0.09	0.818(1)	1.336(2)	1.134(7)	1.343(2)

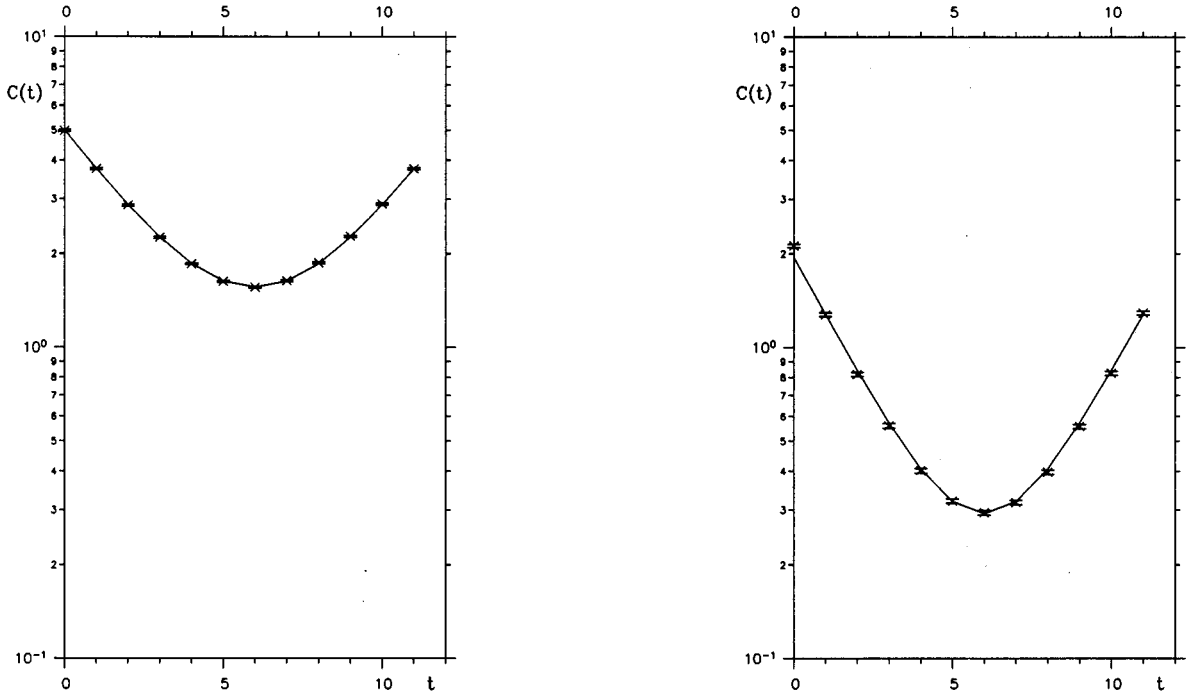

FIG. 12. Correlation functions type 2, $\beta = 0.05$, $m_u = m_d = 0.02$, π_u (left), and π_d (right). Crosses denote positive values of the correlation function, the solid line denotes the fit.

function, 32 local sources distributed over the lattice were used. Masses were determined by fits to the formula:

$$C(t)=A_1(e^{-E_1 t}+e^{-E_1(T-t)})+A_2(-1)^t(e^{-E_2 t}+e^{-E_2(T-t)}) +A_3+(-1)^t A_4. \quad (46)$$

Here, E_1 is the energy of the lightest pseudoscalar and E_2 the energy of the lightest scalar state. The constants A_3 and A_4 correspond to single fermions which propagate in the time direction around the lattice (see [33]). Here, they were not needed for fits of $\overline{uu}$ states in any parameter region investigated. Masses of neutral composite states for $\beta \sim \beta_{cu}$ are presented in Table VIII and for $\beta \sim \beta_{cd}$ in Table IX.

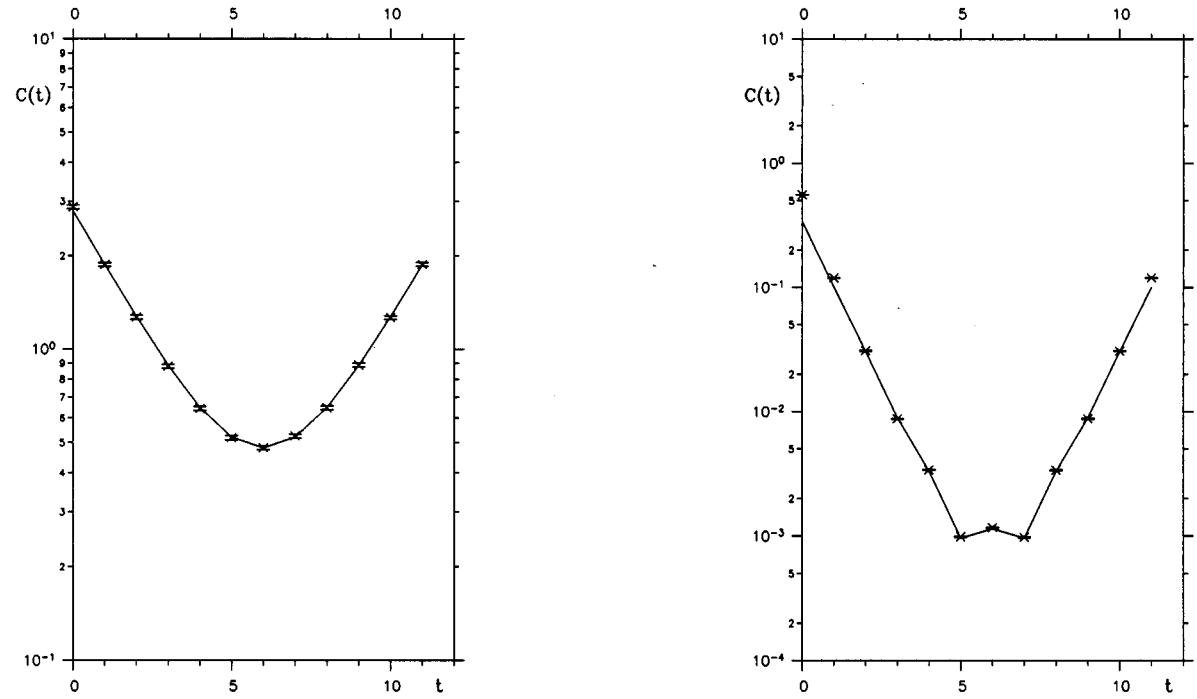

FIG. 13. Correlation functions type 2, $\beta = 0.17$, $m_u = m_d = 0.02$, π_u (left), and π_d (right). The symbols have the same meaning as above.

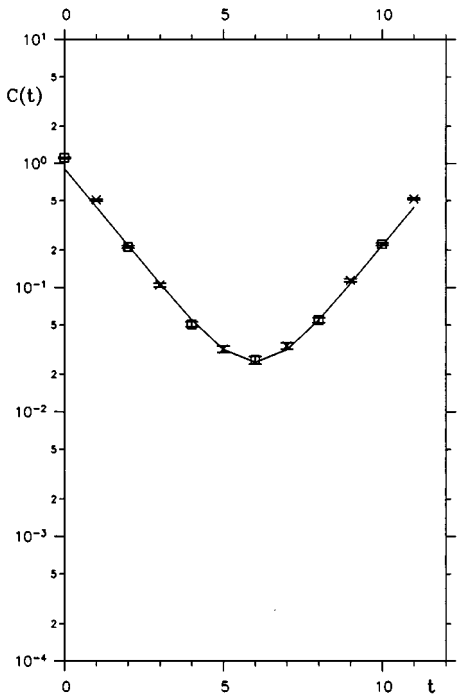

FIG. 14. Correlation functions type 1, $\beta = 0.05$, $m_u = m_d = 0.02$, $\hat{\sigma}_d$. Crosses denote positive and squares negative values of the correlation function, the solid line denotes the fit.

For correlation functions of type 2, fits were done with A_2 set to zero. In this channel, only the Goldstone pion contributes, since states with the quantum numbers 0^{+-} cannot be realized in the quark model. Figure 12 shows correlation functions of type 2 at $\beta \sim \beta_{cd}$ and Fig. 13 at $\beta \sim \beta_{cu}$. For $\overline{uu}$ states, a fit interval $t_{\min}/t_{\max} = 1/11$ was chosen. Close to β_{cd}, the mass of the π_u is nearly independent of the fit interval, which indicates that there is a good overlap of the pointlike interpolating field with the pion. For $\beta \leqslant 0.19$, the masses of the $\overline{uu}$ pions are smaller than $2m_{uR}$, thus one can speak of bound states, which become lighter the deeper one goes into the broken phase. For $\beta \geqslant 0.20$, the π_u masses lie above $2m_{uR}$. This is an indication that the pion is not bound any more; instead there is possibly, in the infinite volume limit, a resonance in the pseudoscalar channel. It has to be noted that when a spectrum with many states is fitted with a single exponential, the fit result might be an average between the lowest-lying state around $2m_R$ and the excited states [33].

For $\overline{dd}$ states, the fit range was at $\beta < 0.10$ chosen to be $t_{\min}/t_{\max} = 1/11$. For larger β, good fits could not be obtained unless the constants A_3 and A_4 were included. A_3 and A_4 are about 10^{-3} smaller than A_1. The fit interval was, in this β range, chosen to be $t_{\min}/t_{\max} = 2/10$. The π_d masses are around β_{cd} below $2m_{dR}$, for $\beta > 0.05$ there is no bound pseudoscalar $\overline{dd}$ state.

Figures 14 and 15 show typical correlation functions of type 1 for couplings close to β_{cu} and β_{cd}. For β values much lower than β_{cu}, there is no clear signal for the $\hat{\sigma}_u$ correlation function. The results shown in Tables VIII and IX were obtained without including the pseudoscalar contribution in the fit. Apparently, the pseudoscalar state does not give any important contribution to correlation functions of type 1, its amplitude is about an order of magnitude smaller than the one of the scalar state and χ^2 per degree of freedom is the same whether the pseudoscalar state is included in the fit or not. The difference in the results from both fits is of the same order as the error because of the choice of the fit interval. Fit intervals were $t_{\min}/t_{\max} = 2/10$. For β values be-

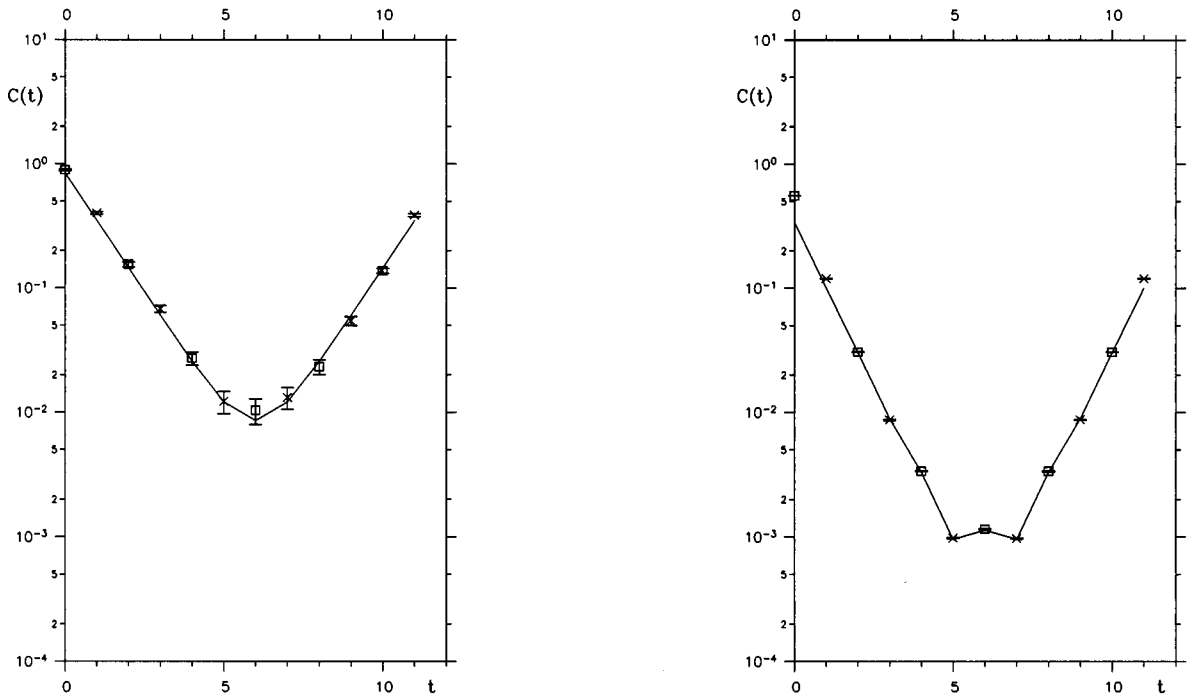

FIG. 15. Correlation functions type 1, $\beta = 0.17$, $m_u = m_d = 0.02$, $\hat{\sigma}_u$ (left), and $\hat{\sigma}_d$ (right). The symbols have the same meaning as above.

tween 0.15 and 0.17, the $\hat{\sigma}_u$ energies lie slightly below $2m_{uR}$ so that they might be bound in this region. For larger β they get larger than twice the renormalized fermion mass. In the parameter region studied, all $\hat{\sigma}_d$ masses are larger than $2m_{dR}$. From the simulation results at $\beta \geq 0.075$, one observes that far in the symmetric phase, π_d and $\hat{\sigma}_d$ states are degenerate, as one would expect from restoration of chiral symmetry.

Correlation functions for charged composite states ($\overline{ud}$) have been calculated for β values around β_{cu}, β_{cd} and for $\beta=0.12$. For small β, the correlation functions suffer from bad noise problems, and the signal appears to fall off with an energy larger than the inverse lattice spacing. For large β there is a good signal, but the correlation function falls off with an energy which is $O(1)$ in lattice units and thus much larger than the sum of the renormalized fermion masses. At $\beta=0.12$, there is a signal in the channel considered and the energy is of the order of m_{uR}. However, the renormalized u mass is large $[O(1)]$ at those values of the coupling and cannot be determined reliably because correlators are very noisy. Thus no evidence for charged bound states, with small energies in the limit of large cutoff, has been found.

B. Renormalization group flows

In Sec. III it was discussed that in the two-charge model, the cutoff cannot be removed if the renormalized coupling is kept finite. In such cases there is always the question if there are parameter regions where physics can be kept fairly constant while the cutoff is changed. In QED with one set of charges, in general flow lines of constant mass ratios involving composite states cross flow lines of constant renormalized charge even before the maximal cutoff resulting from triviality is reached. Only in the sector with very small charges and masses are the flow lines nearly parallel, and physics can be kept nearly constant. There are indications that the situation can be improved if four-fermion interactions are included [21]. In the two-charge model, the two species of fermions interact with each other only weakly and one expects the behavior of flow lines belonging to the d to be completely different from the behavior of those belonging to the u.

The physically most interesting region in the phase diagram is around $\beta \simeq \beta_{cu}$ and at small bare masses. Looking at Table IX, it seems reasonable to assume that energies of composite states of one fermion only have a very small dependence on the bare mass of the other fermion and thus the flow lines in the plane $m \equiv m_u = m_d$ can easily be generalized to the two-dimensional flow surface. To obtain flow lines in the $m_u = m_d$ plane, an interpolation between the grid of actual simulation results in this plane is performed. For this, the dependence of mass ratios S on the simulation parameters is assumed to be as follows:

$$\ln S = a + b\beta, \quad m \text{ fixed}, \tag{47}$$

$$\ln S = c + d \ln m, \quad \beta \text{ fixed}. \tag{48}$$

The ansatz in Eq. (47) is motivated by the logarithmic relation Eq. (35) between renormalized masses and the charge, whereas Eq. (48) is motivated by the scaling behavior expected from the equations of state. Figure 16 shows lines

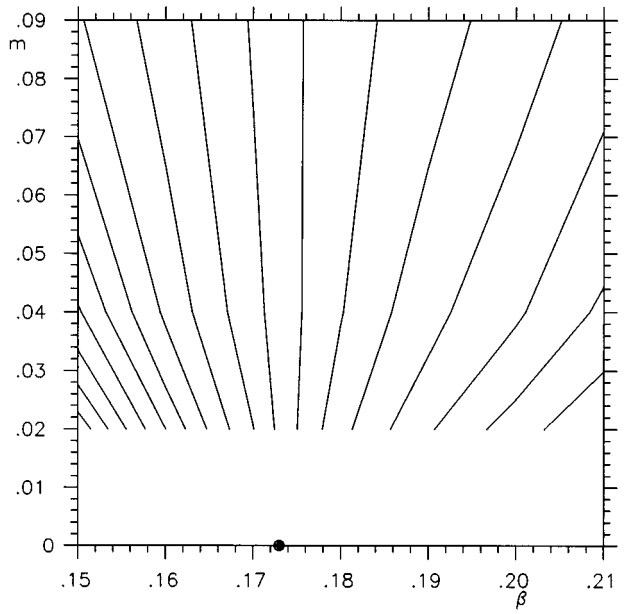

FIG. 16. Lines with constant m_{uR}/m_{π_u} in the $m_u = m_d$ plane. The black dot denotes β_{cu}.

with a constant ratio $S = m_{uR}/m_{\pi_u}$ in the $m_u = m_d$ plane. S is varied in steps of 0.1 from 0.4 to 2.1. The picture suggests that the lines flow into β_{cu}. Generalizing this to different values of m_u and m_d, one obtains a picture about the flows as shown in Fig. 17. Surfaces $S = \text{const}$ are expected to end on the $m_u = 0$ plane at the phase boundary of the u. As the thick black line in Fig. 17 indicates, one generally cannot keep the ratio of fermion and pion masses constant on a line with constant fermion mass ratio and renormalized charge, except probably in the perturbative region.

Figure 18 shows lines with a constant ratio $S = m_{uR}/m_{\hat{\sigma}_u}$. S is varied in steps of 0.025 from 0.3 to 0.6. The lines do not flow into β_{cu}. One expects that lines of constant β_R and fermion mass ratio will also, in general, not lie on the surface one obtains from generalizing S to the three-dimensional parameter space. However, for very small

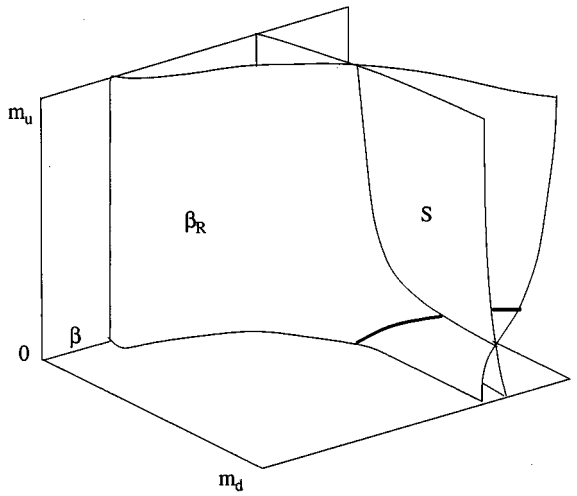

FIG. 17. Sketch of a surface with constant β_R and a surface with constant m_{uR}/m_{π_u}. The thick black line denotes a constant fermion mass ratio on the surface with constant β_R.

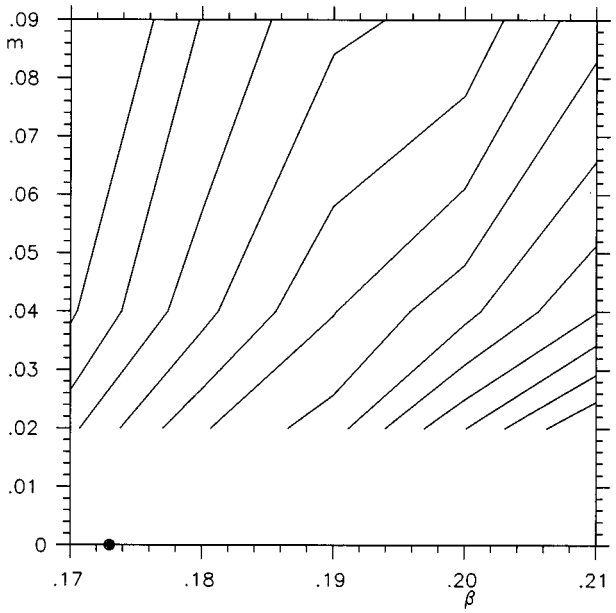

FIG. 18. Lines with constant m_{uR}/m_{σ_u} in the $m_u = m_d$ plane. The black dot denotes β_{cu}.

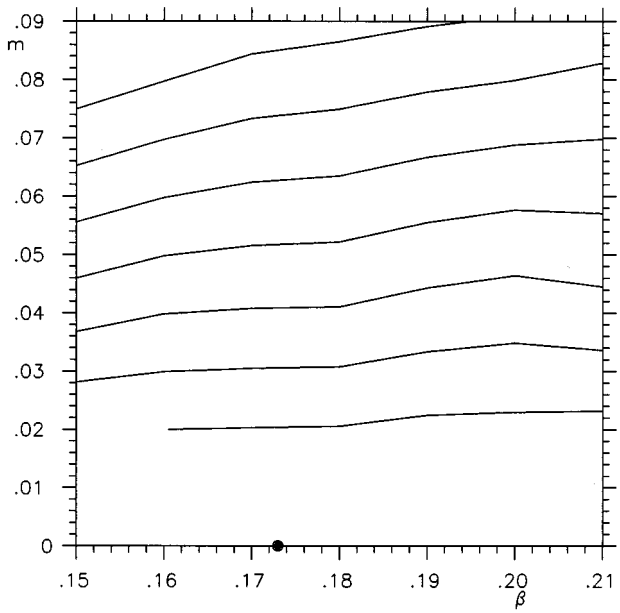

FIG. 19. Lines with constant m_{dR}/m_{π_d} in the $m_u = m_d$ plane. The black dot denotes β_{cu}.

couplings and masses it seems that flow lines with constant coupling and fermion mass ratio follow surfaces with constant mass ratios closely and renormalizability is essentially restored. Lines with constant $S = m_{dR}/m_{\pi_d}$ are shown in Fig. 19. S is varied in steps of 0.0125 from 0.025 to 0.1. The lines show that this mass ratio is, for large couplings, fairly independent of m_d.

V. CONCLUSIONS

In this paper a lattice study of noncompact QED with two sets of staggered fermions with charges 1 (u) and $-1/2$ (d) (''two-charge model''), is presented. The phase diagram is obtained from the chiral condensates. They can be described by a fit with equations of state of an O(2) symmetric linear σ model with logarithmic corrections to the mean-field equations. Chiral symmetry breaking occurs at different values of the bare coupling for both fermions, for the u fermion at $\beta_{cu} = 0.173(1)$ and for the d fermion at $\beta_{cd} = 0.047(1)$. The most interesting candidate for a continuum limit of the model is at β_{cu}, with $m_u = m_d = 0$. This is the end point of the line on the β axis where renormalized masses of both fermions are zero in units of the cutoff. There are indications that for smaller β, the renormalized d mass can go to zero, while the renormalized u mass is finite. If β is lowered past β_{cd}, both renormalized masses are always finite.

The renormalized coupling has been determined and found to be compatible with perturbation theory. Other effects to the charge renormalization, such as possible charged bound states, seem not to give a noticeable contribution. The agreement with perturbation theory indicates that the renormalized charge of all fermions vanishes even if only one becomes massless. An estimate for the validity bound of the two-charge model was obtained and generalized to all charged fermions in the standard model. Including all known charged fermions, one gets an upper bound of $\alpha_R \lesssim 1/80$ if one assumes QED to be valid up to the Planck scale.

Study of composite states ($\overline{uu}$ and dd) has shown that in the neighborhood of the physically interesting point β_{cu}, only the $\overline{uu}$ states are bound. Masses of dd states are $O(1)$ in lattice units in this region of the phase diagram. It appears that because of the shape of renormalization group flows of mass ratios, one cannot keep physics constant even approximately in the investigated parameter region. The theory seems to already become inconsistent at scales which are lower than the cutoff because of triviality. However, there are indications that renormalizability is approximately restored in the perturbative region. The situation that the theory is, in general, not renormalizable, may be improved by including other operators into the action.

ACKNOWLEDGMENTS

I am grateful to G. Schierholz for many inspiring suggestions and would also like to thank R. Horsley, M. Göckeler, P. Rakow, and H. Stüben for valuable discussions. The numerical calculations were performed on the Cray Y-MP at HLRZ Jülich and the Alliant FX2816 at GMD, St. Augustin, and I would like to thank both computer centers for their support. This work was partly supported by SHEFC and the EU under Contract No. EC CHRX-CT92-0051.

[1] L. D. Landau, A. A. Abrikosov, and I. M. Khalatnikov, Dok. Akad. Nauk SSSR **95**, 177 (1954); L. D. Landau and I. Ya. Pomeranchuk, Dok. Akad. Nauk SSSR **102**, 489 (1955); L. D. Landau, in *Niels Bohr and the Development of Physics*, edited by W. Pauli (Pergamon, London, 1955); L. D. Landau, A. A. Abrikosov, and I. M. Khalatnikov, Nuovo Cimento Suppl. **3**, 80 (1956).

[2] R. P. Feynman, in *QED, the Strange Theory of Light and Mat-*

ter (Princeton University Press, Princeton, NJ, 1985), Chap. 4.
[3] V. A. Miransky, Nuovo Cimento A **90**, 149 (1985); Sov. Phys. JETP **61**, 905 (1985); P. I. Fomin, V. P. Gusynin, V. A. Miransky, and Yu. A. Sitenko, Riv. Nuovo Cim. **6**, 1 (1983).
[4] J. Bartholomew, S. H. Shenker, J. Sloan, J. Kogut, M. Stone, H. W. Wyld, J. Shigemitsu, and D. K. Sinclair, Nucl. Phys. **B230** [FS10], 222 (1984).
[5] M. Salmhofer and E. Seiler, Commun. Math. Phys. **139**, 395 (1991); **146**, 637(E) (1992).
[6] K. Kondo and H. Nakatani, Nucl. Phys. **B351**, 236 (1991).
[7] T. Appelquist, D. Karabali, and L. C. R. Wijewardhana, Phys. Rev. Lett. **57**, 957 (1986); K. Yamawaki, M. Bando, and K. Matumoto, *ibid.* **56**, 1335 (1986); M. Bando, T. Morozumi, H. So, and K. Yamawaki, **59**, 389 (1987).
[8] M. Tanabashi, in *Proceedings of the 1991 Nagoya Spring School on Dynamical Symmetry Breaking*, Nagoya, Japan, edited by K. Yamawaki (World Scientific, Singapore, 1991), p. 336.
[9] J. B. Kogut, E. Dagotto, and A. Kocić, Phys. Rev. Lett. **60**, 772 (1988).
[10] J. B. Kogut, E. Dagotto, and A. Kocić, Nucl. Phys. **B317**, 253, 271 (1989).
[11] E. Dagotto, A. Kocić, and J. B. Kogut, Nucl. Phys. **B331**, 500 (1990).
[12] A. Kocić, J. B. Kogut, M.-P. Lombardo, and K. C. Wang, Nucl. Phys. **B397**, 451 (1993).
[13] S. P. Booth, R. D. Kenway, and B. J. Pendleton, Phys. Lett. B **228**, 115 (1989).
[14] M. Göckeler, R. Horsley, E. Laermann, P. Rakow, G. Schierholz, R. Sommer, and U.-J. Wiese, Nucl. Phys. **B334**, 527 (1990).
[15] M. Göckeler, R. Horsley, P. Rakow, G. Schierholz, and R. Sommer, Nucl. Phys. **B371**, 713 (1992).
[16] V. Azcoiti, G. Di Carlo, and A. F. Grillo, Int. J. Mod. Phys. A **8**, 4235 (1993); Phys. Lett. B **305**, 275 (1993).
[17] A. Kocić, in *Lattice '93*, Proceedings of the International Symposium, Dallas, Texas, edited by T. Draper *et al.* [Nucl. Phys. B (Proc. Suppl.) **34**, 123 (1994)].
[18] V. Azcoiti, G. Di Carlo, A. Galante, A. F. Grillo, V. Laliena, and C. Piedrafita, in *Lattice '95*, Proceedings of the International Symposium, Melbourne, Australia in [Nucl. Phys. B (Proc. Suppl.) (in press)], Report No. hep-lat/9509037 (unpublished); V. Azcoiti, G. Di Carlo, A. Galante, A. F. Grillo, V. Laliena, and C. Piedrafita, Phys. Lett. B **353**, 279 (1995).
[19] M. Göckeler, R. Horsley, V. Linke, P. E. L. Rakow, G. Schierholz, and H. Stüben, in *Lattice '94*, Proceedings of the International Symposium, Bielefeld, Germany, edited by F. Karsch *et al.* [Nucl. Phys. B (Proc. Suppl.) **42**, 660 (1995)].
[20] A. M. Horowitz, Phys. Rev. D **43**, R2461 (1991).
[21] P. E. L. Rakow, Nucl. Phys. **B356**, 27 (1991).
[22] K. Bitar, A. D. Kennedy, R. Horsley, S. Meyer, and P. Rossi, Nucl. Phys. **B313**, 348 (1989).
[23] E. Brezin, J. C. Le Guillou, and J. Zinn-Justin, in *Phase Transitions and Critical Phenomena*, edited by C. Domb and M. S. Green (Academic, London, 1976), Vol. 6, p. 125.
[24] G. Schierholz, in *Lattice '90*, Proceedings of the International Symposium, Tallahassee, Florida, edited by U. M. Heller, A. D. Kennedy, and S. Sanielevici, [Nucl. Phys. B (Proc. Suppl.) **20**, 623 (1991)].
[25] A. Ali Khan, in *Lattice '92*, Proceedings of the International Symposium, Amsterdam, The Netherlands, edited by J. Smit and P. van Baal [Nucl. Phys. B (Proc. Suppl.) **30**, 733 (1993)].
[26] M. Göckeler, in *Lattice '90* [24], p. 642.
[27] R. Horsley, M. Göckeler, E. Laermann, P. Rakow, G. Schierholz, R. Sommer, and U.-J. Wiese, in *Lattice '90* [24], p. 639.
[28] M. Lüscher, Nucl. Phys. **B341**, 341 (1990).
[29] M. Göckeler, R. Horsley, E. Laermann, U.-J. Wiese, P. E. L. Rakow, G. Schierholz, and R. Sommer, Phys. Lett. B **251**, 567 (1990); **256**, 562(E) (1991).
[30] A. Ali Khan, Ph.D. thesis (in German), University of Hamburg, 1994 DESY Internal Report No. T–94–02, 1994 (unpublished).
[31] D. E. Müller, *A method for solving algebraic equations using an automatic computer*, Mathematical Tables and Aids to Computation **10**, 208 (1956); B. Leavenworth, *Algorithm 25: Real zeros of an arbitrary function*, Communications of the ACM **3**, 602 (1960).
[32] E. Dagotto, A. Kocić, and J. Kogut, Phys. Lett. B **232**, 235 (1989).
[33] A. Ali Khan, M. Göckeler, R. Horsley, P. E. L. Rakow, G. Schierholz, and H. Stüben, Phys. Rev. D **51**, 3751 (1995).
[34] M. F. L. Golterman, Nucl. Phys. **B273**, 663 (1986).